



Targeting hepatocellular carcinoma: Synthesis of new pyrazole-based derivatives, biological evaluation, DNA binding, and molecular modeling studies



Dina M. Omran^a, Mariam A. Ghaly^{a,*}, Shahenda M. El-Messery^b, Farid A. Badria^c, Ehab Abdel-Latif^d, Ihsan A. Shehata^a

^a Department of Medicinal Chemistry, Faculty of Pharmacy, Mansoura University, Mansoura 35516, Egypt

^b Department of Pharmaceutical Organic Chemistry, Faculty of Pharmacy, Mansoura University, Mansoura 35516, Egypt

^c Department of Pharmacognosy, Faculty of Pharmacy, Mansoura University, Mansoura 35516, Egypt

^d Department of Chemistry, Faculty of Science, Mansoura University, Mansoura 35516, Egypt

ARTICLE INFO

Keywords:

Pyrazole
Synthesis
Anticancer activity
DNA binding
Molecular docking

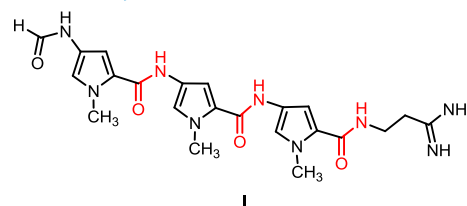
ABSTRACT

A new series of pyrazole derivatives was prepared in this work, including pyrazolopyrimidines, pyrazolotriazines, pyrazolylthienopyridines, and 2-(pyrazolylamino)thiazol-4-ones, utilizing 3-amino-5-methyl-1H-pyrazole as a synthetic precursor. Their *in vitro* anticancer activity was tested on hepatocellular carcinoma cell line, HepG2. The results revealed that the pyrazolylhydrazonoyl cyanide **8**, the pyrazolopyrimidine **3**, and the pyrazolylaminothiazolone **17** were the most active with IC₅₀ values of 2, 7, and 7 μM respectively in comparison with 5.5 μM for cisplatin as a reference drug. Interestingly, all the synthesized compounds showed higher selectivity index than cisplatin. DNA binding assay was also carried out for the synthesized compounds to rationalize their mechanism of action. Molecular modeling studies, including docking into DNA minor groove, flexible alignment, and surface mapping, were conducted. Results obtained proved the superior DNA-binding affinity of the most active anticancer compounds.

1. Introduction

Cancer is ongoing to be a serious health trouble worldwide. According to GLOBOCAN 2018 estimates, cancer new cases and deaths have risen to 18.1 million and 9.6 million respectively in 2018 [1]. Hepatocellular carcinoma is considered as one of the most prevalent cancers and the second leading cause of cancer deaths. Although the mortality rate from other widespread cancers, e.g. lung and breast cancers, is diminishing, the death rate from liver cancer elevated by 2.8% in men and 3.4% in women per year [2]. Despite the great advances made in the chemotherapeutic management of cancer patients, discovering novel efficient anticancer agents, selective on cancerous and less toxic to normal cells, is still one of the hottest areas in medicinal chemistry research. DNA has long been proven to be the most important target in cancer therapy. Generally, DNA interactive drugs include DNA-alkylating agents, DNA intercalators, and DNA groove binders [3]. Interaction of a small molecule with DNA leads to interruption in replication, transcription, and repair, and ultimately killing the fast growing cells [4]. Intercalation and minor groove binding are

considered the most abundant binding modes of small ligands to DNA [5,6]. One of the prototype AT-selective DNA minor groove binders is distamycin (I). It is a natural tripeptide antibiotic containing three methylpyrrole units [7,8].



The majority of clinically used anticancer drugs are derived from nitrogen heterocyclic compounds. Considerable attention has been paid to the pyrazole scaffold as a highly flexible drug-like building block that is widely used in the development of anticancer agents [9–11]. Ruxolitinib and crizotinib (Fig. 1) are examples of pyrazole-containing drugs used for treating myeloproliferative neoplasm and non-small cell lung carcinoma respectively [12]. In addition, Reddy et al. [13]

* Corresponding author.

E-mail address: mariamghaly@mans.edu.eg (M.A. Ghaly).

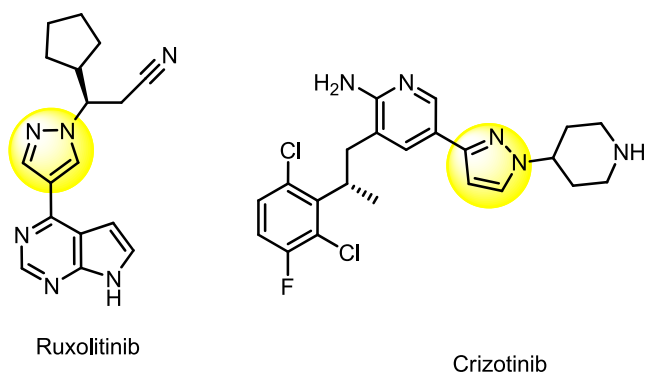


Fig. 1. Examples of pyrazole-containing anticancer drugs.

reported the antiproliferative activities of a series of pyrazolamide-containing compounds, where compound II showed potent cytotoxic activity (Fig. 2). In another study, the *in vitro* cytotoxic activities of a series of substituted thiazolopyrazole derivatives were reported, of which compound III (Fig. 2) was the most potent, showing an IC_{50} value of 0.2 μ M against HepG2 cell line [14]. In a third study, the anticancer activity of a series of trisubstituted pyrazoles against hepatocellular carcinoma (HCC) cell lines was tested. Compound IV, bearing a thiazolyl moiety, was the most active against HCC cell lines used, including HepG2, and had a better activity than the reference drug sorafenib [12].

The incorporation of the pyrazole ring with other biologically active heterocycles, e.g. pyrimidine, has been successfully employed by El-Naggar and co-workers [15] who reported the remarkable activity of the pyrazolopyrimidine derivative V against HepG2 cancer cell lines showing an IC_{50} value less than that of doxorubicin (Fig. 2).

Taking all the above considerations into account, the research reported herein involves the synthesis of a new series of polysubstituted pyrazole-based derivatives, including pyrazolopyrimidines and their isosteric pyrazolotriazines, pyrazolamides, and 2-(pyrazolylamino) thiazol-4-ones (Fig. 2), their *in vitro* anticancer evaluation against HepG2 cell line, and their DNA-binding evaluation. Furthermore, molecular modeling studies, including docking into DNA minor groove,

flexible alignment, and surface mapping were also performed in order to rationalize the experimental data obtained on the basis of computer-aided tools.

2. Results and discussion

2.1. Chemistry

The reaction of 3-amino-5-methyl-1H-pyrazole (1) with ethyl 2-cyano-3,3-bis(methylthio)acrylate (2) [16] has been carried out by heating in DMF to furnish the corresponding 5-amino-7-methylthio-pyrazolo[1,5-a]pyrimidine derivative 3 (Scheme 1). The structure of compound 3 was elucidated based on its compatible spectroscopic data. The absorption of ester carbonyl, at lower frequency (1670 cm^{-1}) rather than the usual absorption in the region 1735 cm^{-1} , is attributed to its formation of intramolecular hydrogen bonding with the next amino group. The ^1H NMR spectrum clearly indicated triplet at δ 1.32 ppm and quartet at δ 4.26 ppm for the ethoxy group ($-\text{OCH}_2\text{CH}_3$). The two singlet signals at δ 2.42 and 2.47 were attributed to the protons of two methyl groups (pyrazole- CH_3 and $-\text{SCH}_3$). The proton of pyrazole-C3 resonated as singlet at δ 6.10 ppm while the protons of amino function resonated as two singlet signals at δ 6.92 and 8.65 ppm. *N,N*-Dimethyl-*N'*-pyrazolylformimidamide derivative 4 has been synthesized by refluxing aminopyrazole 1 with dimethylformamide-dimethylacetal (DMF-DMA) in toluene [17]. Heating of *N,N*-dimethyl-*N'*-pyrazolylformimidamide derivative 4 with malononitrile in ethyl alcohol induced further heterocyclization reaction to afford 7-amino-6-cyanopyrazolo[1,5-a]pyrimidine derivative 5 via elimination of dimethylamine molecule $\text{HN}(\text{CH}_3)_2$. The structure of compound 5 was secured based on its compatible spectroscopic data. The infrared spectrum revealed absorptions at 3293, 3178 and 2222 cm^{-1} to indicate the existence of amino (NH_2) and nitrile ($\text{C}\equiv\text{N}$) groups, respectively. The ^1H NMR spectrum indicated a singlet for one proton at δ 8.25 ppm, which refers to the proton of pyrimidine at the fifth position.

3-Amino-5-methyl-1H-pyrazole (1) was employed as an important precursor for the preparation of pyrazolo[5,1-c]triazine derivatives through its diazotization by sodium nitrite and HCl followed by coupling with various activated nitriles. Thus, the diazocoupling reaction of the pyrazolyl diazonium chloride 6 with 3-iminobutanenitrile (7)

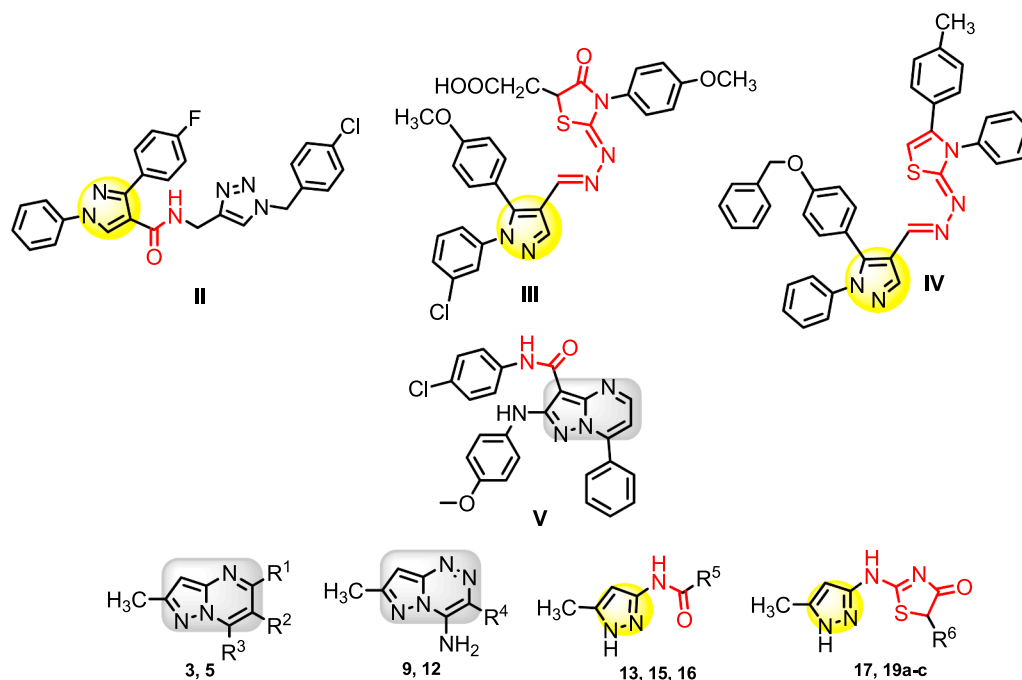
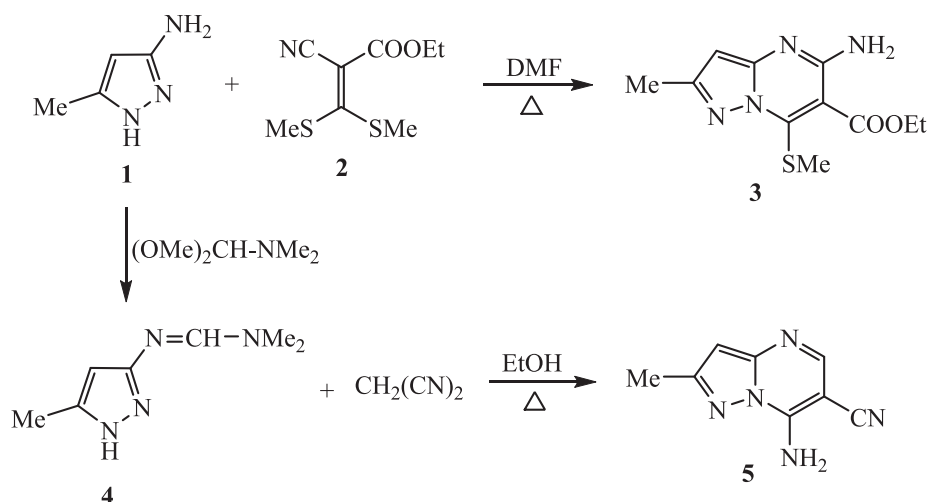
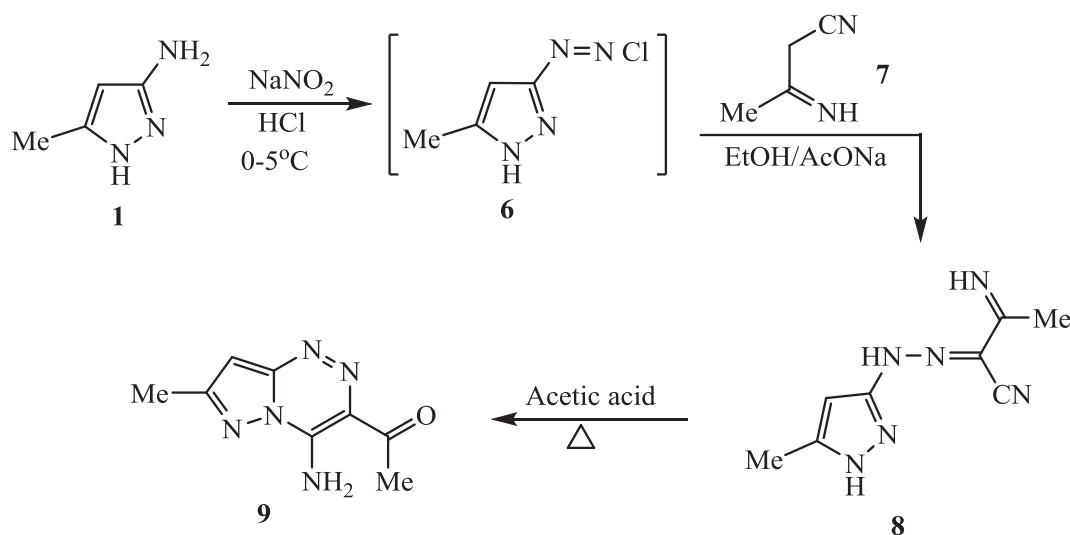


Fig. 2. Examples of pyrazole-containing anticancer compounds and the designed target compounds.



Scheme 1. Synthesis of pyrazolopyrimidines 3 and 5.



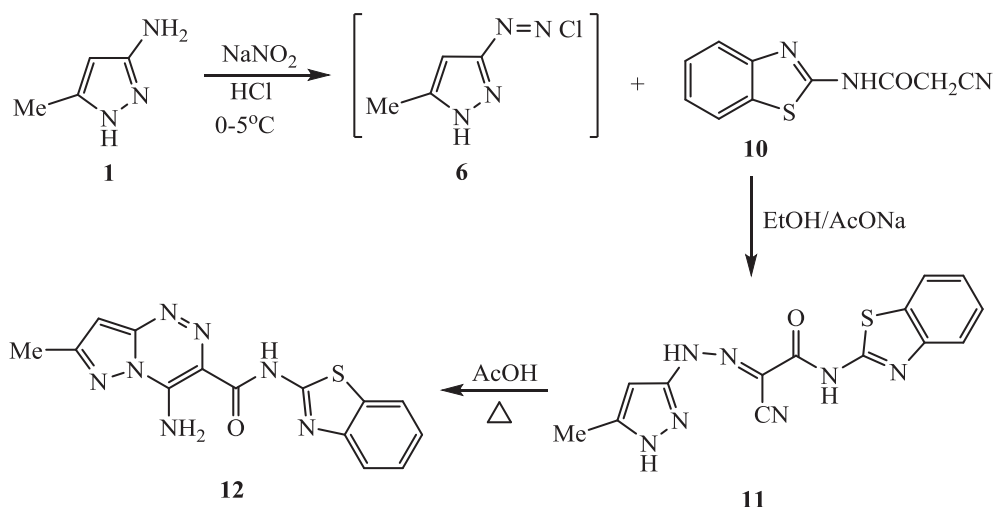
Scheme 2. Synthesis of pyrazolotriazine derivative 9.

was carried out in ethanol and sodium acetate to produce the corresponding hydrazone cyanide **8**, which upon warming in acetic acid gave the corresponding pyrazolo[5,1-*c*]triazine derivative **9** (Scheme 2). The infrared spectrum displayed the absorptions of N–H stretching vibrations at 3392 and 3235 cm^{-1} conforming to the amino function, in addition to the absorption of one carbonyl group at 1661 cm^{-1} . The ^1H NMR signals resonated as singlet at δ 2.50 ppm (pyrazole-CH₃), singlet at δ 2.73 (COCH₃), singlet at δ 6.90 (pyrazole-H8) and two singlet signals at δ 9.11 and 9.30 (NH₂).

In addition, the diazotized aminopyrazole compound **6** has been coupled with benzothiazolyl-cyanoacetamide derivative **10** by stirring in cold ethanol containing sodium acetate to furnish the conforming hydrazone cyanide **11**. This hydrazone was readily cyclized into its pyrazolotriazine derivative **12** by heating in acetic acid (Scheme 3). The chemical structure of **12** was confirmed by spectroscopic techniques including IR and NMR analyses. The infrared absorption at 1663 cm^{-1} clearly indicated the presence of carbonyl-amidic (CONH). The ^1H NMR signals were singlet at δ 2.30 ppm (–CH₃), singlet at δ 6.95 ppm (pyrazole-H4), two singlet signals at δ 8.83 and 9.34 (NH₂) and singlet at δ 12.19 ppm (NH).

Chloroacetylation of 3-aminopyrazole **1** was achieved by stirring with chloroacetyl chloride in the presence of DMF and triethylamine to afford the pyrazolyl-chloroacetamide derivative **13** (Scheme 4). The chemical structure of **13** was confirmed because of its agreeable

spectral data. The presence of infrared absorptions at $\nu = 3249$, 3182 and 1761 cm^{-1} referred to the functional groups N–H and C=O, respectively. The ^1H NMR signal at δ 4.22 ppm that integrated for two protons indicated the presence of methylene group (–COCH₂-Cl). The nucleophilic replacement of chlorine atom from the pyrazolyl-chloroacetamide derivative **13** by different sulfur nucleophiles was investigated. Firstly, nucleophilic substitution of chlorine was tested by the reaction of **13** with 2-mercapto-nicotinonitrile compound **14**; the reaction proceeded in acetone containing anhydrous potassium carbonate to furnish the conforming sulfide compound **15**. This sulfide compound **15** was used as a precursor for the building of its corresponding thieno[2,3-*b*]pyridine derivative **16** through the successful intramolecular cyclization in hot ethanolic sodium ethoxide (Scheme 4). The formation of this thieno[2,3-*b*]pyridine derivative **16** may be interpreted through the nucleophilic addition of the methylene group to nitrile function according to the mechanistic consideration. The structures of these synthesized compounds **15** and **16** were established by agreeable IR and NMR data. The IR spectrum of **15** displayed the absorption band of nitrile group at 2215 cm^{-1} that disappeared from the IR spectrum of **16** as an indication for the cyclization progress. The ^1H NMR spectrum of compound **15** exhibited the two protons of methylene group as singlet signal at δ 4.12 ppm; this signal disappeared from spectrum of the product **16** as additional evidence for the successful cyclization reaction.



Scheme 3. Synthesis of pyrazolotriazine derivative 12.

Moreover, the reaction of pyrazolyl chloroacetamide derivative 13 with ammonium thiocyanate has been carried out in boiling ethanol to afford 2-((5-methyl-1H-pyrazol-3-yl)amino)thiazol-4(5H)-one (17) which finds support from its correct spectral data (Scheme 5). The infrared absorption at 1722 cm^{-1} assigned the carbonyl group of the thiazol-4-one ring. The cyclic methylene group of the thiazol-4-one ring resonated as singlet (^1H NMR spectrum) for two protons at δ 3.91 ppm. The constructed thiazol-4-one derivative 17 was condensed with three benzaldehyde derivatives 18 (namely, 4-toulaldehyde, 4-anisaldehyde and 4-nitrobenzaldehyde) in glacial CH_3COOH and anhydrous CH_3COONa (Knoevenagel condensation reaction) furnished the corresponding 5-arylidene-2-((5-methyl-1H-pyrazol-3-yl)amino)thiazol-4(5H)-one derivatives 19a-c. The infrared absorption of these thiazolones 19a-c in the region $1700\text{--}1707\text{ cm}^{-1}$ clearly indicated the presence of carbonyl-thiazolone ring. The ^1H NMR signals of 19b (as an example) were singlet at δ 2.23 ppm (pyrazole- CH_3), singlet at δ 3.81 ppm ($-\text{OCH}_3$), singlet at δ 5.89 ppm (pyrazole-H4), two doublet at δ 7.10 and 7.65 ppm (aromatic-H) and singlet for two protons at δ 12.24 ppm (2NH).

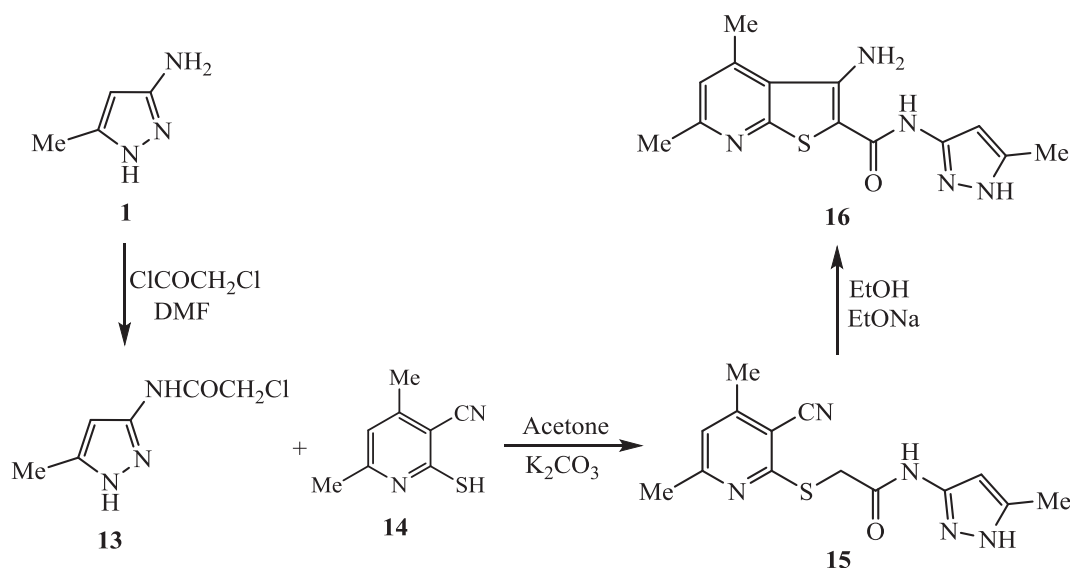
2.2. Biological evaluation

2.2.1. Cytotoxicity assay

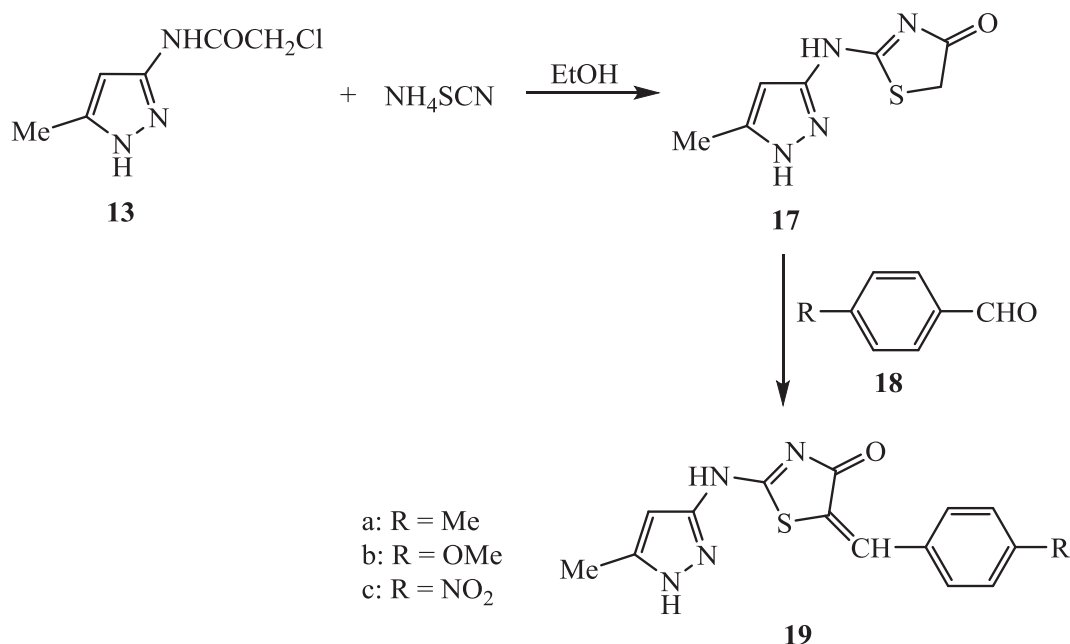
Fourteen compounds were tested *in vitro* against hepatocellular carcinoma cell line (HepG2). Interestingly, all the tested compounds revealed a higher selectivity index (SI) than cisplatin as a reference drug (SI = 0.91). In particular, compounds 3, 8, and 17 exhibited notable cytotoxicity against HepG2 with IC_{50} values of 7, 2, and $7\text{ }\mu\text{M}$, respectively, in comparison with $5.5\text{ }\mu\text{M}$ for cisplatin, in addition to $\text{SI} > 2$ (Table 1).

2.2.2. DNA-binding assay

DNA represents the target of many small molecules that bind it and proved to be effective anticancer drugs. Various strategies have been used to study the interaction of these small molecular weight compounds with DNA. Methyl green in particular works by reversibly binding to DNA, producing a colored complex stable at neutral pH, while unbound methyl green fades. The DNA-binding active candidate displaces methyl green from its DNA complex. A spectroscopic assay



Scheme 4. Synthesis of pyrazolylthienopyridine derivative 16.



Scheme 5. Synthesis of 5-arylidene-2-(pyrazolylamino)-thiazol-4-one derivatives **19a-c**.

Table 1

The cytotoxic activity and selectivity of the synthesized compounds against hepatocellular carcinoma (HepG2) cell line.

Compound	HepG2 (IC ₅₀ , μM) ^{**}	VERO-B (IC ₅₀ , μM) ^{**}	SI [*]
3	7 ± 0.40	15.001 ± 0.10	2.14
4	40 ± 0.50	50.007 ± 0.32	1.25
5	40 ± 0.50	50.003 ± 0.40	1.25
8	2 ± 0.03	9.000 ± 0.05	4.50
9	40 ± 0.50	50.002 ± 0.07	1.25
11a	12 ± 1.5	30.001 ± 0.02	2.50
12a	40 ± 0.50	50.008 ± 0.15	1.25
13	40 ± 0.50	50.007 ± 0.02	1.25
15	11.8 ± 0.20	26.000 ± 0.03	2.20
16	12 ± 1.5	30 ± 0.20	2.50
17	7 ± 0.40	15 ± 0.17	2.14
19a	50 ± 0.30	60 ± 0.25	1.20
19b	50 ± 0.30	60 ± 0.04	1.20
19c	40 ± 0.50	50 ± 0.03	1.25
Positive Control	5.5 ± 1.5	5 ± 0.11	0.91

* SI: Selectivity Index.

** Values represent the concentration (mean ± SD, n = 3–5 separate determinations).

could determine this displacement through measuring the absorbance decrease at 630 nm [18].

Table 2 showed that compounds **3**, **8**, and **17** displaced methyl green from DNA and bound to DNA with % of displacement at 80%, 90%, and 80% respectively.

2.3. Molecular modeling studies

2.3.1. Molecular docking study

Molecular modeling studies have been introduced in this work as a valuable tool to rationalize the DNA binding results obtained experimentally. Binding modes of ligands to DNA usually include intercalation between adjacent base pairs or intrusion into the minor or the major groove [19].

To get a better image, the molecular structures of both the active compounds **8**, **3**, and **17**, and inactive counterparts **19a** and **19b**, in a comparative modeling study style, were constructed and overviewed at DNA binding site. At the beginning of the work, conformational

Table 2

Effect of synthesized compounds on the displacement activity for methyl green from DNA (DNA-binding assay).

Compound	% of Methyl Green Displacement
3	80.98 ± 0.40
4	47.77 ± 0.03
5	49.91 ± 0.12
8	90.41 ± 0.31
9	48.64 ± 0.24
11a	66.63 ± 0.14
12a	56.57 ± 0.11
13	49.52 ± 0.27
15	69.33 ± 0.110
16	66.24 ± 0.20
17	80.27 ± 0.13
19a	30.50 ± 0.07
19b	39.53 ± 0.18
19c	50.31 ± 0.32
Doxorubicin (Standard)	97.22 ± 0.01

* Values represent the concentration (mean ± SD, n = 3–5 separate determinations) required for a 50% decrease in the initial absorbance of the DNA methyl green solution.

analysis of the target compounds were obtained using the MM force-field [20] followed by (calculations in vacuo, bond dipole option for electrostatics using PolakRibiere algorithm, and RMSD gradient of 0.15 kcal/Å mol) implemented in MOE, 2009.10 [21].

The lowest energy conformers of the most active DNA binders **8**, **3**, and **17**, were represented in Fig. 3a,b,c while Fig. 3d,e showed the lowest conformers of inactive candidates **19a** and **19b** respectively. The X-ray crystallographic structure of DNA dodecamer d(CGCAAATTTGCG) conjugated with a bifurcated hydrogen-bonded conformation of the AT base pairs with its complexed distamycin A was obtained from the Protein Data Bank (PDB code: 2DND) and used for the docking study [22].

Fig. 4 showed the binding mode of distamycin reference. It was bound to DNA bases adenine, cytosine, and thiamine via hydrogen bonding network interactions by 79%, 67% and 88% respectively with a calculated binding energy of −11.3452 kcal/Å mol.

Compounds **8**, **3**, and **17** were selected in our modeling study as active DNA binding agents. Alignment of these derivatives against

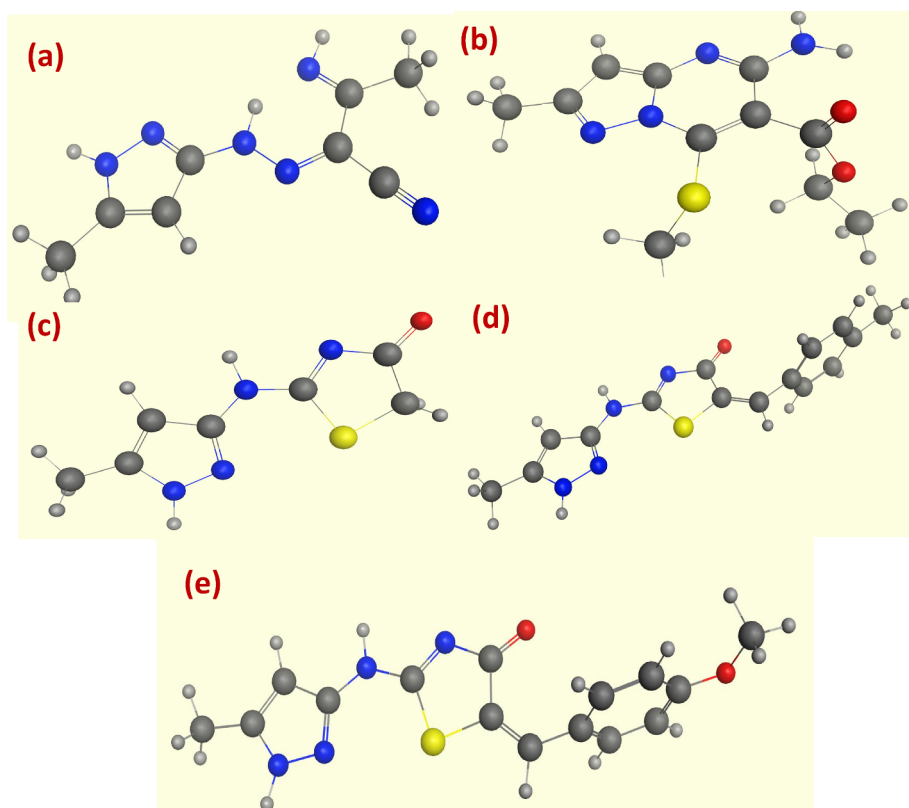


Fig. 3. Lowest energy conformers of active compounds (a) **8**, (b) **3**, (c) **17**, and the least active compounds (d) **19a** and (e) **19b** in balls and cylinders.

distamycin reference was conducted. The results were shown (Fig. 5a–c) where it was obvious the high alignment between the active DNA binders and distamycin. Moreover, their overall shape oriented along the minor groove in a curved manner which in major part interprets their DNA binding activity.

The binding mode of these compounds were also under focus, where a remarkable note was detected. These compounds simply manifested a binding mode (hydrogen bonding) similar to distamycin which may account for their higher activity. Compound **8** showed triad hydrogen bonding mode via 16%, 91%, and 78% with binding energy of -10.4489 kcal/Å mol (Fig. 6a). Compound **3** had the hydrogen bonding in bi mode by 42% and 66% with a binding affinity of -10.2834 kcal/Å mol (Fig. 6b). Compound **17** binding mode occurred via double interaction by 13% and 94% with binding affinity of

-9.9987 kcal/Å mol (Fig. 6c) (DNA base pairs were omitted in previous figures for simplicity). On the contrary, docking study of inactive DNA binders represented by **19a**, **19b** obviously exhibited a different binding mode into DNA minor groove. Both of them were not well hosted into the DNA bases, and did not show any hydrogen bonding to them (Fig. 7a,b).

Such clear contrast between the tested active and inactive candidates has interpreted the difference in biological response of these compounds into DNA double strand and showed the importance of hydrogen bonding in stabilizing the binding interactions.

2.3.2. Flexible alignment

Alignment of compounds at the active site is a known technique to structurally analyse protein ligand complexes. A good alignment is

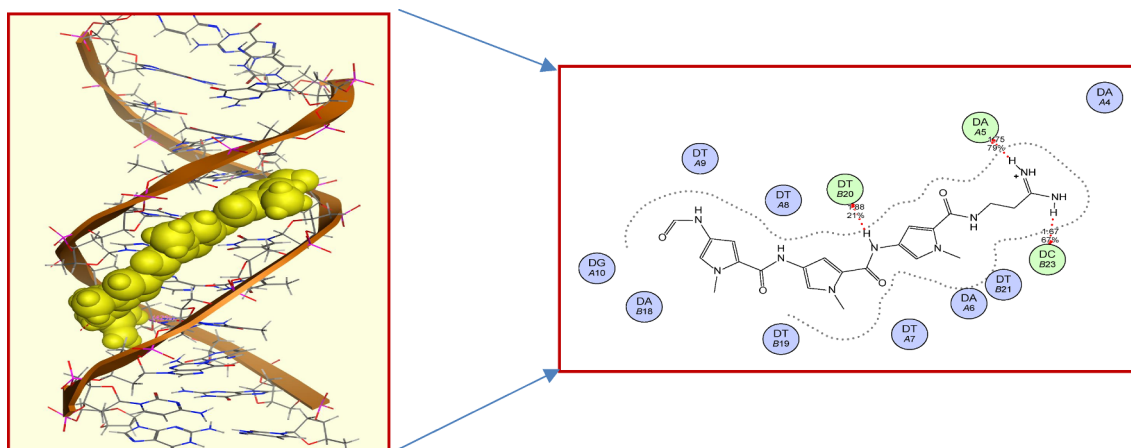


Fig. 4. (a) Distamycin, shown in yellow space filled form lying in between DNA base pairs, DNA shown in ribbon form. (b) DNA minor groove binding of distamycin (yellow) with DNA in 2D form. (For interpretation of the references to colour in this figure legend, the reader is referred to the web version of this article.)

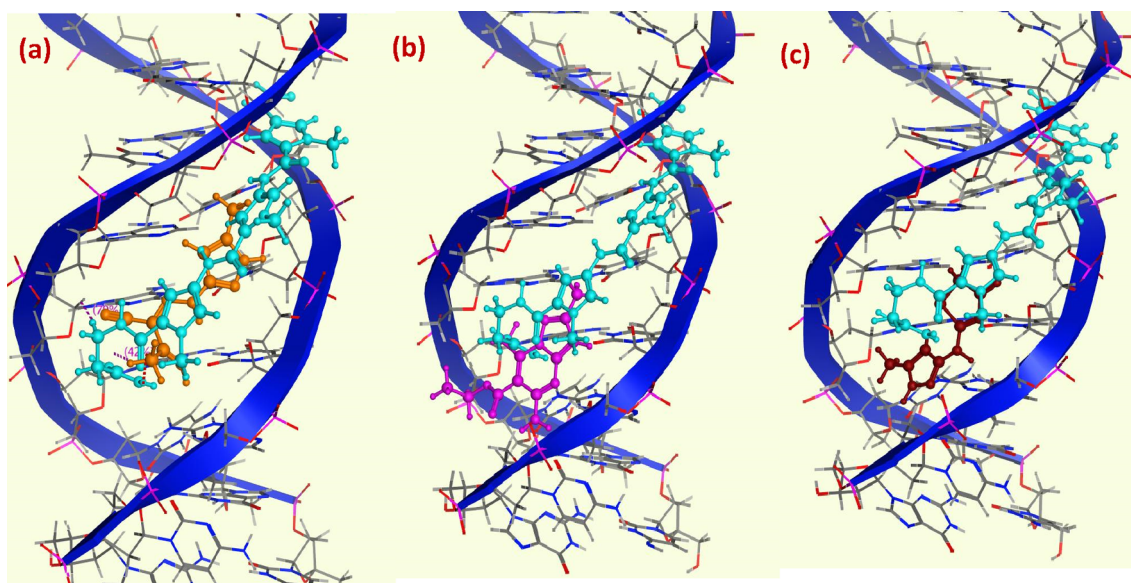


Fig. 5. Sketches of minimized and docked structures in the DNA (blue ribbon) revealing overlay of distamycin (cyan) in duplex together with: (a) **8** (orange), (b) **3** (pink) and (c) **17** (brown). (For interpretation of the references to colour in this figure legend, the reader is referred to the web version of this article.)

achieved when the strain energy of each molecule is small along with occurrence of similar shape and aromatic atoms overlapping between compounds [23]. Triple flexible alignment experiments have been performed. Firstly, that experiment was conducted using three active candidates **8**, **3**, and **17** against each other through generation of the lowest energy of 200 conformers for each compound, minimization by a distance dependent dielectric model, then selection of a low energy set of 100 for further analysis. In Fig. 8a, a higher alignment score was calculated with the least strain energy which represents a better alignment score. Secondly, the same experiment was done using the two chosen inactive derivatives **19a** and **19b** which again showed higher matching, Fig. 8b. Finally, the alignment experiment was repeated using both active and inactive candidates represented by **8** and

19b which, as expected, showed recognized deviation from alignment pattern ensuring and illustrating that their biological activity are different.

2.3.3. Surface mapping

For further investigating the different activity patterns of the tested compounds, a surface mapping study was conducted [24]. At first, surface mapping of active candidate **8** was created (Fig. 9a) followed by surface hydrophobic mapping of inactive counterpart compound **19b** (Fig. 9b). Compound **8** showed more greener areas on the map indicating more hydrophobic regions, while the inactive compound **19b** showed a different surface mapping distribution with less green coloration indicating higher hydrophilic feature of the whole molecule.

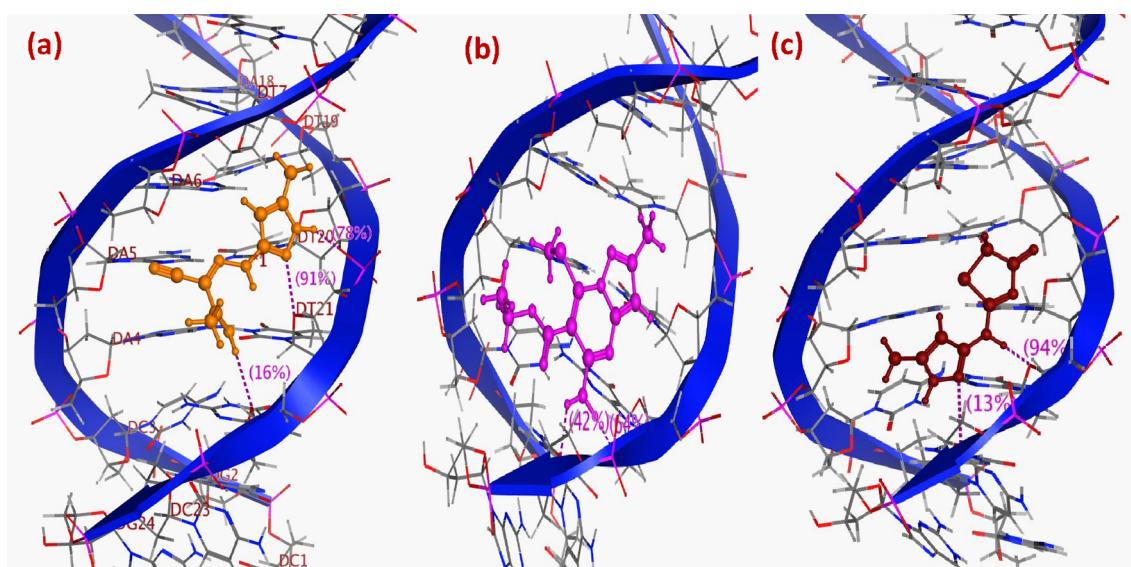


Fig. 6. DNA minor groove binding of (a) **8** (orange), (b) **3** (pink), and (c) **17** (brown). DNA is shown in ribbon form. Investigated compounds are shown in ball and cylinder form. Hydrogen-bonding (HB) interactions with the DNA bases are shown in dashed lines. Numbers indicate the percent of HB. (For interpretation of the references to colour in this figure legend, the reader is referred to the web version of this article.)

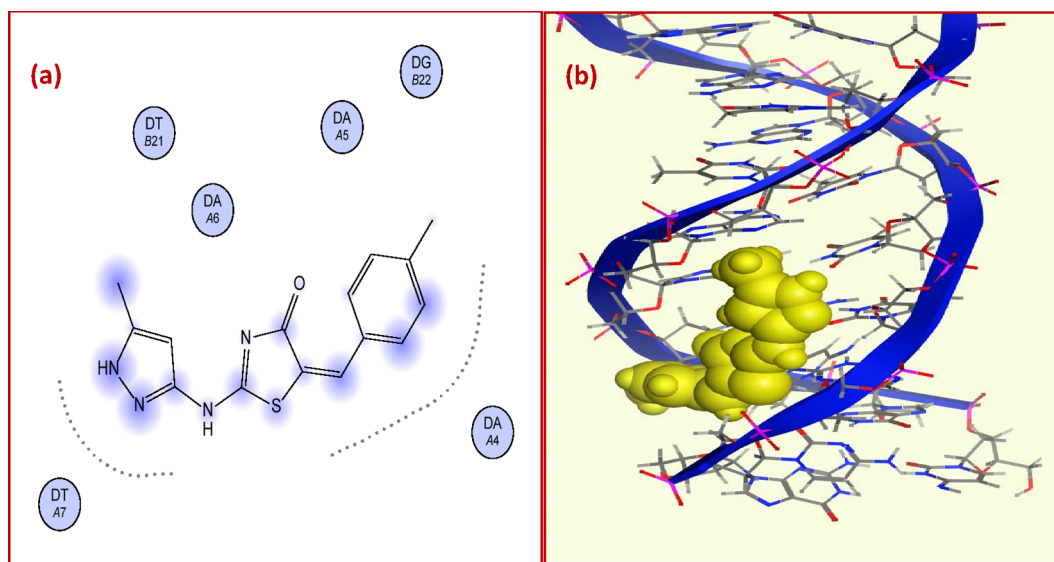


Fig. 7. (a) 2D binding mode and residues involved in the recognition of **19a**. (b) Close-up view of inactive candidate **19b** binding in the DNA minor groove, highlighting the conformation of DNA active out of minor groove.

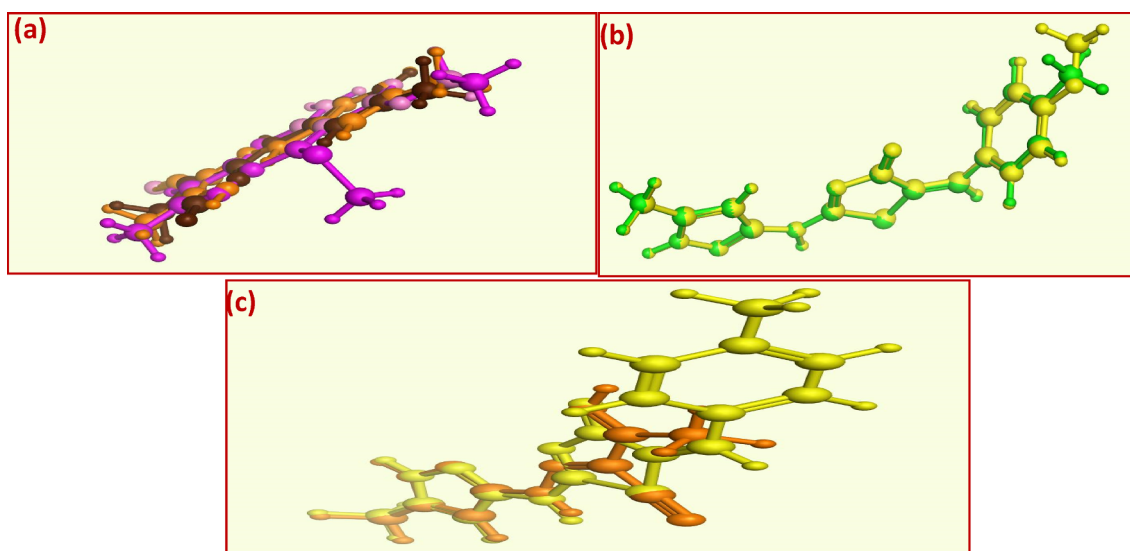


Fig. 8. (a) Flexible alignment of active DNA binders **8** (orange), **3** (pink), and **17** (brown). (b) Flexible alignment of inactive DNA binders **19a** (yellow) and **19b** (green). (c) Flexible alignment of active DNA binders **8** (orange) and inactive one **19b** (yellow). (For interpretation of the references to colour in this figure legend, the reader is referred to the web version of this article.)

Comparing the two figures (Fig. 9a,b) obviously confirms the different patterns of the compounds of interest providing additional explanation for their different DNA binding activity.

3. Conclusion

In this study, a new series of polysubstituted pyrazole-based derivatives was synthesized and evaluated for anticancer activity against hepatocellular carcinoma. DNA binding assay was also performed for the synthesized compounds to rationalize their mechanism of action. Results obtained proved the superior DNA-binding affinity of compounds **8**, **3**, and **17**. Molecular modeling studies, including docking into DNA minor groove, flexible alignment, and surface mapping were carried out. The results were in accordance with the experimental results, providing additional explanation for the DNA-binding activity of the most active anticancer compounds. The results obtained proved the unique character, high selectivity and promising activity of several tested compounds against aggressive liver cancer cell line HepG2,

particularly, compound **8**, making it a promising anticancer candidate that could be combined with commonly used chemotherapeutic drugs aiming to improve the tumor response. A more strict *in vivo* study could be undertaken to reveal more preclinical data such as bioavailability, pharmacokinetics, and oral stability with expectation of good activity and high safety.

4. Experimental protocols

4.1. Chemistry

Melting points are uncorrected and measured on Gallenkamp electric apparatus. The IR spectra were recorded on a Thermo Scientific Nicolet iS10 FTIR spectrometer. The NMR spectra were determined using a Bruker WP 300 spectrometer at 300 MHz for ^1H NMR or 100 MHz for ^{13}C NMR. The MS analysis was carried on a Quadrupole GC/MS Thermo Scientific Focus/DSQII at 70 eV. Elemental analyses (C, H and N) were determined on Perkin-Elmer 2400 analyzer.

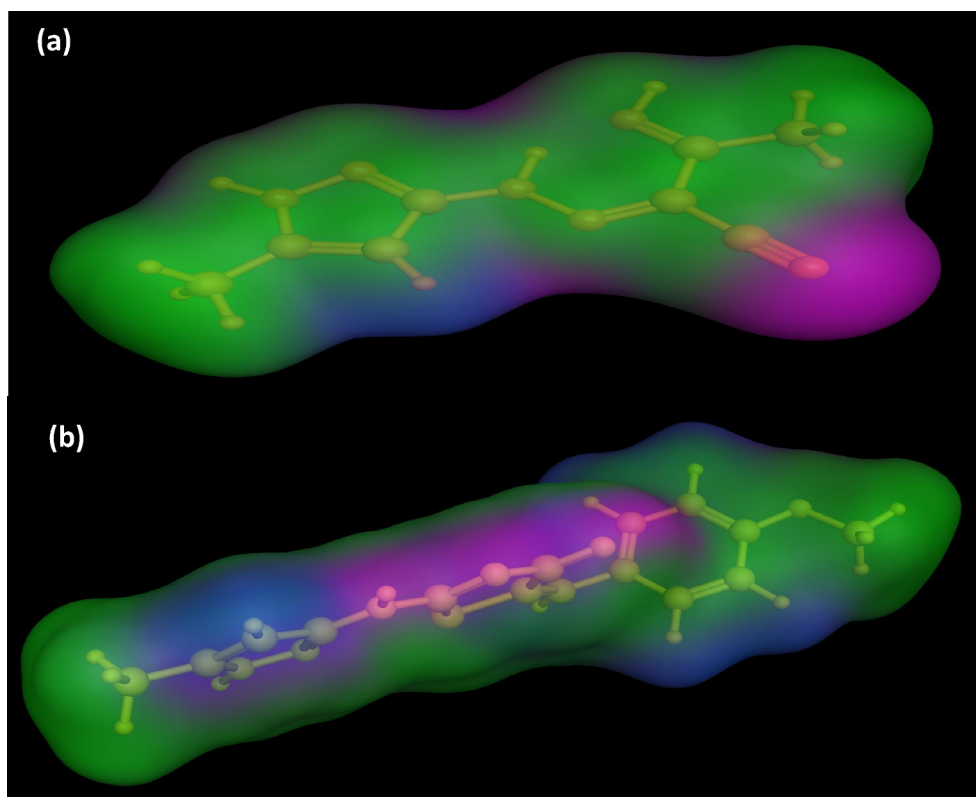


Fig. 9. (a) Surface map for the most active compound **8** in the pocket side. (b) Surface map for the least active compound **19b** in the pocket side. Green: hydrophobic, blue: mild polar, pink: hydrophilic.

4.1.1. Synthesis of 5-amino-6-ethoxycarbonyl-2-methyl-7-methylthio-pyrazolo [1,5-a]pyrimidine (**3**)

To a suspension of 3-amino-5-methyl-1H-pyrazole (**1**) (2 mmol, 0.19 g) in 15 ml DMF, ethyl 2-cyano-3,3-bis(methylthio)acrylate (**2**) (2 mmol, 0.43 g) was added and boiled under reflux for 4 hrs. The solid that separated upon dilution with 20 ml cold water was picked up by filtration. Recrystallization of the filtered solid was achieved by heating in ethanol.

Yellow solid, yield = 64%, m.p. = 191–193 °C. IR ($\nu_{\max}/\text{cm}^{-1}$): 3374, 3263 (–NH₂), 1670 (C=O). ¹H NMR (CDCl₃): δ 1.32 (t, $J = 7.15$ Hz, 3H), 2.42 (s, 3H), 2.47 (s, 3H, SCH₃), 4.26 (q, $J = 7.15$ Hz, 2H), 6.10 (s, 1H, pyrazole-H3), 6.92 (s) and 8.65 (s) (2H, NH₂). ¹³C NMR (DMSO-*d*₆): δ 9.66, 9.90, 10.04, 56.55, 84.38, 90.88, 142.75, 144.31, 151.59, 157.87, 162.43. Analysis for C₁₁H₁₄N₄O₂S (266.32): Calcd: C, 49.61; H, 5.30; N, 21.04%. Found: C, 49.43; H, 5.36; N, 21.15%.

4.1.2. Synthesis of *N,N*-dimethyl-*N'*-(5-methyl-1H-pyrazol-3-yl)-formimidamide (**4**)

To a solution of 3-amino-5-methyl-1H-pyrazole (**1**) (10 mmol, 0.97 g) in 15 ml toluene, DMF-DMA (10 mmol, 1.2 ml) was added and refluxed for 4 hrs. The solid obtained upon cooling was filtered and recrystallized from ethyl alcohol.

White solid, yield = 86%, m.p. = 122–123 °C, lit. m.p. 120–122 °C [17]. IR ($\nu_{\max}/\text{cm}^{-1}$): 3204 (N–H), 1636 (C=N). ¹H NMR (DMSO-*d*₆): δ 2.19 (s, 3H), 2.86 (s, 3H), 2.97 (s, 3H), 6.22 (s, 1H, pyrazole-H4), 8.12 (s, 1H, N=CH), 10.39 (s, 1H, NH). ¹³C NMR (DMSO-*d*₆): δ 11.82, 34.41 (2C), 96.15, 155.02, 158.86, 162.68. Analysis for C₇H₁₂N₄ (152.20): Calcd: C, 55.24; H, 7.95; N, 36.81%. Found: C, 55.40; H, 7.91; N, 36.89%.

4.1.3. Synthesis of 7-amino-6-cyano-2-methylpyrazolo[1,5-a]pyrimidine (**5**)

A suspension of *N,N*-dimethyl-*N'*-pyrazol-3-yl-formimidamide **4** (3 mmol, 0.45 g) and malononitrile (3 mmol, 0.20 g) was refluxed in

ethyl alcohol for 2 hrs. The solid obtained upon cooling was picked up by filtration and then dried.

White solid, yield = 68%, m.p. = 240–242 °C. IR ($\nu_{\max}/\text{cm}^{-1}$): 3293, 3178 (NH₂), 2222 (C≡N), 1674 (C=N). ¹H NMR (DMSO-*d*₆): δ 2.41 (s, 3H), 6.39 (s, 1H, pyrazole-H3), 8.25 (s, 1H, pyrimidine-H5), 8.81 (s, 2H, NH₂). ¹³C NMR (DMSO-*d*₆): δ 14.75, 73.14, 97.71, 116.67, 149.51, 151.42, **155.85**. MS (*m/z*, %): 173 (100.00), 120 (18.03), 108 (8.53). Analysis for C₈H₇N₅ (173.18): Calcd: C, 55.48; H, 4.07; N, 40.44%. Found: C, 55.34; H, 4.10; N, 40.55%.

4.1.4. Synthesis of *N*-(5-methyl-1H-pyrazol-3-yl)-hydrazono-yl cyanides **8** and **11**

A well-stirred suspension of **1** (10 mmol, 0.97 g) in conc. HCl (3 ml) was cooled in ice bath and diazotized with NaNO₂ solution (10 mmol, 0.70 g). The obtained cold solution was slowly added to a well-stirred solution of 3-iminobutanenitrile **7** (10 mmol, 0.82 g) and/or benzothiazolyl-cyanoacetamide derivative **10** (10 mmol) in 30 ml ethanol and 3 g of sodium acetate. The reaction mixture was stirred for an hour and then kept in refrigerator for 12 h. The solid obtained was filtered, washed with 5 ml cold ethanol and dried to pick the hydrazono-yl cyanides **8** and **11**.

4.1.5. 2-Imino-*N*-(5-methyl-1H-pyrazol-3-yl)propanehydrazono-yl cyanide (**8**)

Yellow solid, yield = 46%, m.p. = 128–130 °C. IR ($\nu_{\max}/\text{cm}^{-1}$): 3324, 3135 (N–H), 2235 (C≡N). ¹H NMR (CDCl₃): δ 2.68 (s, 3H), 3.05 (s, 3H), 7.20 (s, 1H, pyrazole-H4), 7.28 (s, 1H, NH). Analysis for C₈H₁₀N₆ (190.21): Calcd: C, 50.52; H, 5.30; N, 44.18%. Found: C, 50.31; H, 5.36; N, 44.30%.

4.1.6. 2-(Benzothiazol-2-ylamino)-*N*-(5-methyl-1H-pyrazol-3-yl)-2-oxoacetohydrazono-yl cyanide (**11**)

Reddish brown solid, yield = 66%, m.p. = 156–157 °C. IR ($\nu_{\max}/$

cm^{-1}): 3332, 3293, 3199 (N–H), 2219 (C≡N), 1662 (C=O). ^1H NMR (CDCl_3): δ 2.60 (s, 3H), 6.89 (s, 1H, pyrazole-H4), 7.36–7.88 (m, 4H), 8.70 (s, 1H), 8.79 (s, 1H). Analysis for $\text{C}_{14}\text{H}_{11}\text{N}_7\text{OS}$ (325.35): Calcd: C, 51.68; H, 3.41; N, 30.14%. Found: C, 51.54; H, 3.37; N, 30.20%.

4.1.7. Synthesis of 4-amino-7-methylpyrazolo[5,1-c][1,2,4]triazines **9** and **12**

A suspension of hydrazoneyl cyanides **8** and/or **11** (3 mmol) was heated in 10 ml acetic acid for half an hour. The solid obtained upon cooling was filtered and dried to furnish the pyrazolotriazines **9** and/or **12**.

4.1.8. 3-Acetyl-4-amino-7-methylpyrazolo[5,1-c][1,2,4]triazine (**9**)

Brown solid, yield = 42%, m.p. = 280–281 °C. IR ($\nu_{\text{max}}/\text{cm}^{-1}$): 3392, 3235 (NH_2), 1661 (C=O). ^1H NMR ($\text{DMSO}-d_6$): δ 2.50 (s, 3H), 2.73 (s, 3H), 6.90 (s, 1H, pyrazole-H8), 9.11 (s, 1H), 9.30 (s, 1H). ^{13}C NMR ($\text{DMSO}-d_6$): δ 14.74, 26.98, 98.33, 125.21, 141.00, 144.17, 149.67, 157.20. Analysis for $\text{C}_8\text{H}_{10}\text{N}_6$ (191.19): Calcd: C, 50.26; H, 4.74; N, 36.63%. Found: Calcd: C, 50.45; H, 4.71; N, 36.76%.

4.1.9. 4-Amino-N-(benzo[d]thiazol-2-yl)-7-methylpyrazolo[5,1-c][1,2,4]-triazine-3-carboxamide (**12**)

Brown solid, yield = 56%, m.p. = 258–259 °C. IR ($\nu_{\text{max}}/\text{cm}^{-1}$): 3443, 3346 (NH and NH_2), 1663 (C=O). ^1H NMR ($\text{DMSO}-d_6$): δ 2.30 (s, 3H, CH_3), 6.95 (s, 1H, pyrazole-H4), 7.34 (t, 1H), 7.47 (t, 1H), 7.80 (d, 1H), 8.03 (d, 1H), 8.83 (s, 1H), 9.34 (s, 1H), 12.19 (s, 1H, NH). ^{13}C NMR ($\text{DMSO}-d_6$): δ 14.75, 98.58, 116.24, 117.90, 121.13, 122.18, 123.72, 126.70, 147.37, 149.11, 151.18, 157.14, 161.22, 172.50. MS (m/z , %): 325 (7.31), 297 (4.04), 216 (27.21), 176 (100.00), 149 (53.73), 122 (58.77). Analysis for $\text{C}_{14}\text{H}_{11}\text{N}_7\text{OS}$ (325.35): Calcd: C, 51.68; H, 3.41; N, 30.14%. Found: C, 51.84; H, 3.47; N, 30.03%.

4.1.10. Synthesis of 3-chloroacetamido-5-methyl-1H-pyrazole (**13**)

To a cold suspension of **1** (10 mmol, 0.97 g) and anhydrous K_2CO_3 (10 mmol, 1.38 g) in 20 ml dry acetone, chloroacetyl chloride (15 mmol, 1.2 ml) was added drop by drop. The reaction mixture was stirred for 4 h and then diluted with 50 ml ice-cold water. The solid formed was filtered and recrystallized from ethyl alcohol.

White solid, yield = 82%, m.p. = 118–120 °C. IR ($\nu_{\text{max}}/\text{cm}^{-1}$): 3249, 3182 (N–H), 1761 (C=O), 1665 (C=N). ^1H NMR (CDCl_3): δ 2.62 (s, 3H), 4.22 (s, 2H), 5.85 (s, 1H), 6.82 (s, 1H, pyrazole-H4), 11.95 (s, 1H). ^{13}C NMR ($\text{DMSO}-d_6$): δ 14.51, 42.49, 104.07, 148.63, 155.36, 165.91. Analysis for $\text{C}_6\text{H}_8\text{ClN}_3\text{O}$ (173.60): Calcd: C, 41.51; H, 4.65; N, 24.21%. Found: C, 41.58; H, 4.62; N, 24.29%.

4.1.11. Synthesis of 2-((3-cyano-4,6-dimethylpyridin-2-yl)thio)-N-(5-methyl-1H-pyrazol-3-yl)acetamide (**15**)

To a stirred suspension of pyridine-2-thiol derivative **14** (10 mmol 1.64 g) and anhydrous K_2CO_3 (10 mmol, 1.38 g) in 40 ml acetone, 3-chloroacetamido-5-methyl-1H-pyrazole (**13**) (10 mmol, 1.73 g) was added. The reaction mixture was refluxed for two hrs and then allowed to cool to room temperature. The solid, obtained after dilution by 20 ml cold water, was filtered and dried. Recrystallization of the crude product was achieved by heating in ethyl alcohol.

Yellow solid, yield = 60%, m.p. = 144–145 °C. IR ($\nu_{\text{max}}/\text{cm}^{-1}$): 3329 (N–H), 2215 (C≡N), 1728 (C=O). ^1H NMR ($\text{DMSO}-d_6$): δ 2.17 (s, 3H), 2.40 (s, 3H), 2.43 (s, 3H), 4.12 (s, 2H), 6.18 (s, 1H, pyrazole-H4), 7.09 (s, 1H, pyridine-H5), 10.64 (s, 1H, NH), 11.59 (s, 1H, NH). Analysis for $\text{C}_{14}\text{H}_{15}\text{N}_5\text{OS}$ (301.37): Calcd: C, 55.80; H, 5.02; N, 23.24%. Found: C, 55.91; H, 5.06; N, 23.15%.

4.1.12. Synthesis of 3-amino-4,6-dimethyl-N-(5-methyl-1H-pyrazol-3-yl)-thieno[2,3-b]pyridine-2-carboxamide (**16**)

The prepared acetamide derivative **15** (3 mmol, 0.90 g) was refluxed for an hour in sodium ethoxide solution (prepared by dissolving 0.10 g sodium metal in 20 ml ethanol). The reaction mixture was

poured into cold water and neutralized with HCl. The precipitate that formed was filtered, dried and recrystallized from 30 ml ethanol to give the conforming thieno[2,3-b]pyridine compound **16**.

White solid, yield = 48%, m.p. = 210–211 °C. IR ($\nu_{\text{max}}/\text{cm}^{-1}$): 3341, 3187 (NH_2 and N–H), 1658 (C=O). ^1H NMR ($\text{DMSO}-d_6$): δ 2.21 (s, 3H), 2.56 (s, 3H), 2.68 (s, 3H), 6.25 (s, 1H, pyrazole-H4), 6.92 (s, 1H, NH_2), 7.01 (s, 1H, pyridine-H5), 9.82 (s, 1H). ^{13}C NMR ($\text{DMSO}-d_6$): δ 11.71, 19.87, 24.15, 103.83, 121.02, 122.68, 125.38, 137.83, 143.62, 147.41, 154.44, 156.02, 159.00, 160.04. Analysis for $\text{C}_{14}\text{H}_{15}\text{N}_5\text{OS}$ (301.37): Calcd: C, 55.80; H, 5.02; N, 23.24%. Found: C, 55.68; H, 5.08; N, 23.35%.

4.1.13. Synthesis of 2-((5-methyl-1H-pyrazol-3-yl)amino)thiazol-4(5H)-one (**17**)

To a suspension of chloroacetamido-pyrazole derivative **13** (10 mmol, 1.73 g) in 20 ml ethanol, ammonium thiocyanate (15 mmol, 1.14 g) was added and boiled under reflux for 5 hrs. The solid obtained upon cooling was filtered and recrystallized from ethanol to furnish the thiazolone derivative **17**.

Yellow solid, yield = 67%, m.p. = 225–226 °C. IR ($\nu_{\text{max}}/\text{cm}^{-1}$): 3276, 3136 (N–H), 1722 (C=O). ^1H NMR ($\text{DMSO}-d_6$): δ 2.19 (s, 3H, CH_3), 3.91 (s, 2H, CH_2), 5.78 (s, 1H, pyrazole-H4), 11.54 (s, 1H), 11.94 (s, 1H). ^{13}C NMR ($\text{DMSO}-d_6$): δ 11.36, 35.98, 97.84, 139.55, 152.19, 161.92, 177.40. Analysis for $\text{C}_7\text{H}_8\text{N}_4\text{OS}$ (196.23): Calcd: C, 42.85; H, 4.11; N, 28.55%. Found: C, 42.98; H, 4.06; N, 28.46%.

4.1.14. Synthesis of 2-((5-methyl-1H-pyrazol-3-yl)amino)-5-arylidene-thiazol-4(5H)-one derivatives **19a-c**

To a suspension of thiazol-4-one derivative **17** (3 mmol, 0.59 g) in 15 ml glacial CH_3COOH , the appropriate para-substituted benzaldehyde derivative (3 mmol) and 0.5 g of fused CH_3COONa were added and then boiled under reflux for 4 h. The reaction mixture was poured onto ice-water, the obtained solid was picked up by filtration and recrystallized from ethyl alcohol.

4.1.15. 2-((5-Methyl-1H-pyrazol-3-yl)amino)-5-(4-methylbenzylidene)-thiazol-4(5H)-one (**19a**)

Yellow solid, yield = 59%, m.p. = 144–145 °C. IR ($\nu_{\text{max}}/\text{cm}^{-1}$): 3218, 3138 (N–H), 1707 (C=O). ^1H NMR ($\text{DMSO}-d_6$): δ 2.23 (s, 3H), 2.36 (s, 3H), 5.89 (s, 1H, pyrazole-H4), 7.15 (d, 1H, NH), 7.36 (d, 2H), 7.50 (d, 2H), 7.62 (s, 1H, olefinic C=CH), 12.36 (s, 2H, 2NH). ^{13}C NMR ($\text{DMSO}-d_6$): δ 11.29, 21.52, 116.88, 125.29, 126.94, 129.64, 129.78, 130.43 (4C), 131.47, 133.28, 140.28, 165.21. Analysis for $\text{C}_{15}\text{H}_{14}\text{N}_4\text{OS}$ (298.36): Calcd: C, 60.38; H, 4.73; N, 18.78%. Found: C, 60.26; H, 4.77; N, 18.68%.

4.1.16. 5-(4-Methoxybenzylidene)-2-((5-methyl-1H-pyrazol-3-yl)amino)-thiazol-4(5H)-one (**19b**)

Yellow solid, yield = 44%, m.p. = 161–163 °C. IR ($\nu_{\text{max}}/\text{cm}^{-1}$): 3214, 3135 (N–H), 1706 (C=O). ^1H NMR ($\text{DMSO}-d_6$): δ 2.23 (s, 3H, CH_3), 3.81 (s, 3H, OCH_3), 5.89 (s, 1H, pyrazole-H4), 7.10 (d, 2H), 7.55 (d, 2H), 7.65 (s, 1H, olefinic C=CH), 12.24 (s, 2H, 2NH). ^{13}C NMR ($\text{DMSO}-d_6$): δ 11.26, 55.92, 98.63, 115.29 (2C), 126.72, 129.81, 131.88 (2C), 137.41, 147.73, 151.74, 156.07, 160.90, 168.36. Analysis for $\text{C}_{15}\text{H}_{14}\text{N}_4\text{O}_2\text{S}$ (314.36): Calcd: C, 57.31; H, 4.49; N, 17.82%. Found: C, 57.47; H, 4.54; N, 17.73%.

4.1.17. 2-((5-Methyl-1H-pyrazol-3-yl)amino)-5-(4-nitrobenzylidene)-thiazol-4(5H)-one (**19c**)

Reddish brown solid, yield = 56%, m.p. = 204–205 °C. IR ($\nu_{\text{max}}/\text{cm}^{-1}$): 3364, 3148 (N–H), 1700 (C=O). ^1H NMR ($\text{DMSO}-d_6$): δ 2.22 (s, 3H, CH_3), 5.89 (s, 1H, pyrazole-H4), 7.65 (s, 1H, olefinic C=CH), 7.81 (d, 2H), 8.33 (d, 2H), 12.48 (s, 2H, 2NH). ^{13}C NMR ($\text{DMSO}-d_6$): δ 11.22, 99.44, 119.12, 124.73 (2C), 127.19, 130.72, 130.84, 131.06 (2C), 140.67, 147.46, 148.57, 172.44. Analysis for $\text{C}_{14}\text{H}_{11}\text{N}_5\text{O}_3\text{S}$ (329.33): Calcd: C, 51.06; H, 3.37; N, 21.27%. Found: C, 51.28; H, 3.30; N, 21.14%.

4.2. Biological evaluation

4.2.1. Cytotoxicity assay

The cytotoxic activity of the synthesized compounds was tested against hepatocellular carcinoma cell line (HepG2). African green monkey kidney cells (Vero-B) were used as normal cells to examine the selectivity toward cancer cells. HepG2 cell line was obtained from the American Type Culture Collection (ATCC). The cells were cultivated at 37 °C and 10% CO₂ in DMEM (Lonza, Germany) medium supplied with 10% fetal bovine serum (Lonza, Germany), 100 IU/ml penicillin and 100 µg/ml streptomycin (Lonza, Germany). Cisplatin (*cis*-diamineplatinum (II) dichloride) was obtained from Sigma-Aldrich and used as a positive control. It was dissolved in 0.9% saline and stored as an 8 mM stock solution at -20 °C. The tested compounds were dissolved in DMSO and stored at -20 °C. The cells' viability was quantified by measuring the activity of mitochondrial succinate dehydrogenase in viable cells using 3-(4,5-dimethylthiazol-2-yl)-2,5-diphenyl tetrazolium bromide (MTT) [25,26].

The cells were seeded in 96-well plates at a concentration of 5×10^4 cells/ml (100 µl/well) and incubated overnight at 37 °C and 5% CO₂. A serial dilution of the tested compounds or cisplatin was then added. DMSO (0.1%) was used as a negative control. The cells were incubated for 48 h, followed by addition of 15 µl of MTT (5 mg/ml in PBS) to each well and further incubation for additional 4 h. Formazan crystals were dissolved by 100 µl acidified SDS solution (10% SDS/0.01 N HCl in PBS). After 14 h of incubation at 37 °C and 5% CO₂, the absorbance was measured using a BioTek microplate reader at 570 nm. Every experiment was repeated three times and a standard deviation (SD ±) was calculated. IC₅₀ was calculated as the concentration that caused 50% inhibition of cell growth. The growth of the cells was monitored and the images were obtained by Gx microscopes (GXMGXD202 Inverted Microscope) at 10x magnification.

Selectivity index was calculated by the following equation: $SI = IC_{50 \text{ normal}} / IC_{50 \text{ cancer}}$, where IC₅₀ normal and IC₅₀ cancer are the concentration of the tested compound that killed 50% of normal cells and of cancer cells respectively.

4.2.2. DNA binding assay

Methyl green solution was prepared as follows; a 2% methyl green (MG) stock solution was prepared by using methylene chloride extraction to remove any impurities of crystal violet. Briefly, an aqueous 4% MG solution was separated several times with methylene chloride until no traces of violet stain could be seen by using a separation funnel and discarding the lower phase (methylene chloride).

A 10 µg/ml MG solution was mixed with 100 µg/ml calf thymus DNA in displacement buffer (0.05 M Tris-HCl, pH 7.5 containing 7.5 mM MgSO₄) and stirred at 37 °C for 24 h. In the next day, 50 µl containing the corresponding IC₅₀ (Table 1) of each compound or the standard drug doxorubicin, dissolved in DMSO, were added to 150 µl of ethanol in each well of the 96-well plate. Ethanol was evaporated overnight in front of a fan. 60 µl of DNA/MG solution were then transferred to each well. The plate was incubated for 24 h covered from light and the absorbance was then measured using a Biotek plate reader. Ethanol was used as a negative control.

The displacement activity for each compound of MG from DNA was calculated using the following equation: Displacement activity = $100 - ((A_{\text{test}}/A_{\text{ethanol}}) * 100)$, where A_{test} and A_{ethanol} are the absorbance of the test compound and of methyl green in presence of ethanol respectively at λ₆₅₀ nm.

4.3. Molecular modeling studies

4.3.1. Conformational analysis

Initial structures for the active compounds **8**, **3**, **17** and the inactive compounds **19a** and **19b** were constructed using the MOE 2009.10. Their energy minima were determined by a semi-empirical method

AM1 (as implemented in MOE, 2009.10). Polake–Ribiere algorithm and Root Mean Square Deviation (RMSD) gradient of 0.01 kcal/mol conformational searching in torsional space was carried out using the multiconformer method.

4.3.2. Docking study

The 3D structures in their neutral forms of the selected derivatives, which represented the most and least active compounds, were built using the MOE of Chemical Computing Group Inc software. The global-minimum (the lowest energy conformer) of each of them was docked into DNA double strands code ID 2DND, obtained from the Protein Data Bank of Brookhaven National Laboratory.

All the hydrogens were added to a refinement protocol in which the constraints on the enzyme were gradually removed and minimized till reaching a 0.01 kcal/mol/Å RMSD gradient. Energy minimization was performed using 'AMBER' molecular mechanics force field. For each ligand, energy minimizations were carried out using 1000 steps of steepest descent, followed by conjugate gradient minimization to a RMSD energy gradient of 0.01 Kcal/mol/Å. Energy of binding was calculated [27,28]. The alpha triangle placement method and the London dG scoring method were used for docking. DNA-ligand complexes were minimized using the MMFF94x force field, till reaching a 0.1 kcal/mol/Å RMSD gradient.

4.3.3. Flexible alignment and surface mapping

The investigated compounds underwent flexible alignment and surface mapping experiments using 'Molecular Operating Environment' software (MOE of Chemical Computing Group Inc., on a Core i7 workstation). Optimization of their geometry was achieved using the MMFF94x forcefield followed by a flexible alignment using systematic conformational search to identify the lowest energy aligned conformation(s) [29,30].

References

- [1] F. Bray, J. Ferlay, I. Soerjomataram, R.L. Siegel, L.A. Torre, A. Jemal, Global cancer statistics 2018: GLOBOCAN estimates of incidence and mortality worldwide for 36 cancers in 185 countries, *CA Cancer J. Clin.* 68 (2018) 394–424.
- [2] S. Chacko, S. Samanta, A novel approach towards design, synthesis and evaluation of some Schiff base analogues of 2-aminopyridine and 2-aminobenzothiazole against hepatocellular carcinoma, *Biomed. Pharmacother.* 89 (2017) 162–176.
- [3] A.A. Almaqwashi, T. Paramanathan, I. Rouzina, M.C. Williams, Mechanisms of small molecule-DNA interactions probed by single-molecule force spectroscopy, *Nucleic Acids Res.* 44 (2016) 3971–3988.
- [4] G.L. Patrick, *An Introduction to Medicinal Chemistry*, 4th ed., Oxford University Press, 2009, p. 119.
- [5] W. Huang, Y. Liu, J. Wang, X. Yuan, J.-R. Cui, Small-molecule compounds targeting the STAT3 DNA-binding domain suppress survival of cisplatin-resistant human ovarian cancer cells by inducing apoptosis, *Eur. J. Med. Chem.* 157 (2018) 887–897.
- [6] M. Lelle, C. Freidel, S. Kaloyanova, I. Tabujew, K. Peneva, Overcoming drug resistance by cell-penetrating peptide-mediated delivery of a doxorubicin dimer with high DNA-binding affinity, *Eur. J. Med. Chem.* 130 (2017) 336–345.
- [7] G.L. Olsen, E. Louie, G.P. Drobny, S.Th. Sigurdsson, Determination of DNA minor groove width in distamycin-DNA complexes by solid-state NMR, *Nucleic Acids Res.* 31 (2003) 5084–5089.
- [8] S. Boga, D. Bouzada, D.G. Pena, M.V. Lopez, M.E. Vazquez, Sequence-specific DNA recognition with designed peptides, *Eur. J. Org. Chem.* (2018) 249–261.
- [9] A. Rahmouni, S. Souiei, M.A. Belkacem, A. Romdhane, J. Bouajila, H.B. Jannet, Synthesis and biological evaluation of novel pyrazolopyrimidines derivatives as anticancer and anti-5-lipoxygenase agents, *Bioorg. Chem.* 66 (2016) 160–168.
- [10] G.M. Nitulescu, C. Draghici, O.T. Olaru, L. Matei, A. Loana, L.D. Dragu, C. Bleotu, Synthesis and apoptotic activity of new pyrazole derivatives in cancer cell lines, *Bioorg. Med. Chem.* 17 (2015) 5799–5808.
- [11] T.S. Reddy, H. Kulhari, V.G. Reddy, V. Bansal, A. Kamal, R. Shukla, Design, synthesis and biological evaluation of 1,3-diphenyl-1H-pyrazole derivatives containing benzimidazole skeleton as potential anticancer and apoptosis inducing agents, *Eur. J. Med. Chem.* 101 (2015) 790–805.
- [12] M.F. Harras, R. Sabour, Design, synthesis and biological evaluation of novel 1,3,4-trisubstituted pyrazole derivatives as potential chemotherapeutic agents for hepatocellular carcinoma, *Bioorg. Chem.* 78 (2018) 149–157.
- [13] V.G. Reddy, T.S. Reddy, V.L. Nayak, B. Prasad, A.P. Reddy, A. Ravikumar, S. Taj, A. Kamal, Design, synthesis and biological evaluation of *N*-((1-benzyl-1H-1,2,3-triazol-4-yl)methyl)-1,3-diphenyl-1H-pyrazole-4-carboxamides as CDK1/ Cdc2 inhibitors, *Eur. J. Med. Chem.* 122 (2016) 164–177.

- [14] E.S. Nossier, S.M. El-Hallouty, E.R. Zaki, Synthesis, anticancer evaluation and molecular modeling of some substituted thiazolidinonyl and thiazolyl pyrazole derivatives, *Int. J. Pharm. Sci.* 7 (2015) 353–359.
- [15] M.E. El-Naggar, A.S. Hassan, H.M. Awad, M.F. Mady, Design, synthesis and anti-tumor evaluation of novel pyrazolopyrimidines and pyrazoloquinazolines, *Molecules* 23 (2018) 1249–1268.
- [16] Z.T. Huang, X. Shi, Synthesis of heterocyclic ketene *N*, *S*-acetals and their reactions with esters of α , β -unsaturated acids, *Synthesis* 2 (1990) 162–167.
- [17] F. Al-Omran, Studies with 1-functionally substituted alkylbenzotriazoles: An efficient route for the synthesis of 1-azolylbenzotriazoles, benzotriazolylazines and benzotriazolylazoloazines, *J. Het. Chem.* 37 (2000) 1219–1223.
- [18] N.S. Burres, A. Frigo, R.R. Rasmussen, J.B. McAlpine, A colorimetric microassay for the detection of agents that interact with DNA, *J. Nat. Prod.* 55 (1992) 1582–1587.
- [19] X. Han, X. Gao, Sequence specific recognition of ligand-DNA complexes studied by NMR, *Curr. Med. Chem.* 8 (2001) 551–581.
- [20] F.C. Bernstein, T.F. Koetzle, G.J. Williams, E.F. Meyer Jr, M.D. Brice, J.R. Rodgers, O. Kennard, T. Shimanouchi, M. Tasumi, The protein data bank: A computer-based archival file for macromolecular structures, *J. Mol. Biol.* 112 (1977) 535–542.
- [21] **Molecular Operating Environment software 10.2009 (MOE) provided with chemical computing group, Canada.**
- [22] M. Coll, C.A. Frederick, A.H. Wang, A. Rich, A bifurcated hydrogen-bonded conformation in the d(A.T) base pairs of the DNA dodecamer d(CGCAAATTTGCG) and its complex with distamycin, *Proc. Natl. Acad. Sci. USA* 84 (1987) 8385–8389.
- [23] M. Ayman, S.M. El-Messery, E.E. Habib, S.T. Al-Rashood, A.A. Almezhia, H.M. Alkahtani, G.S. Hassan, Targeting microbial resistance: Synthesis, antibacterial evaluation and modeling study of new chalcone-based dithiocarbamate derivatives, *Bioorg. Chem.* 85 (2019) 282–292.
- [24] G.S. Hassan, S.M. El-Messery, A. Abbas, Synthesis and anticancer activity of new thiazolo[3,2-*a*]pyrimidines: DNA binding and molecular modeling study, *Bioorg. Chem.* 74 (2017) 41–52.
- [25] T. Mosmann, Rapid colorimetric assay for cellular growth and survival: application to proliferation and cytotoxicity assays, *J. Immunol. Methods* 65 (1983) 55–63.
- [26] T.F. Slater, B. Sawyer, U. Strauli, Studies on succinate-tetrazolium reductase systems. III. Points of coupling of four different tetrazolium salts, *Biochim. Biophys. Acta* 77 (1963) 383–393.
- [27] N.L. Allinger, Conformational analysis. 130. MM2. A hydrocarbon forcefield utilizing V1 and V2 torsional terms, *J. Am. Chem. Soc.* 99 (1977) 8127–8134.
- [28] S. Profeta, N.L. Allinger, Molecular mechanics calculations on aliphatic amines, *J. Am. Chem. Soc.* 107 (1985) 1907–1918.
- [29] S.K. Kearsley, G.M. Smith, An alternative method for the alignment of molecular structures: Maximizing electrostatic and steric overlap, *Tetrahedron Comput. Methodol.* 3 (1990) 615–633.
- [30] P. Labute, C. Williams, M. Feher, E. Sourial, J.M. Schmidt, Flexible alignment of small molecules, *J. Med. Chem.* 44 (2001) 1483–1490.